Analytic Models for Nonlaminated Active Magnetic Thrust Bearings

Zachary Whitlow [a], Carl Knospe [b], Roger Fittro [b]

[a] Helmerich & Payne International Drilling Co., Tulsa, Oklahoma, USA, zwhitlow@gmail.com
[b] University of Virginia, Department of Mechanical & Aerospace Engineering, Charlottesville, VA, USA, rlf9w@virginia.edu

***Abstract*—Analytic models for solid cylindrical electromagnetic actuators are extended to include geometries with a center hole, the configuration typical of thrust-type active magnetic bearings. These models describe the relationship between perturbation to coil current and the variations in mechanical force that result. The models are explicitly dependent on geometric and material properties of the actuator and include the effects of eddy currents, which determine the actuator bandwidth. These models are verified by comparison to high-fidelity finite element results.**

I. INTRODUCTION

Active magnetic bearings (AMB) require little maintenance, are more efficient than traditional mechanical bearings, and may be configured to meet a wide range of design constraints. For these reasons magnetic bearings are frequently incorporated into pumps and compressors used in pipelines, refineries, and even subsea production applications. Radial magnetic bearings are typically laminated to reduce eddy currents and extend the bandwidth of force in response to changes in current. However, due to manufacturing and material constraints, magnetic thrust bearings are usually solid. As a result eddy currents typically have a profound effect on their dynamic response. Zhu et al. developed an analytic model for solid cylindrical magnetic actuators, including eddy current effects, that defines the dynamic relationship between current and mechanical force [1], [2]. This model was modified and extended in a simplified transfer function form by Sun et al. for solid cylindrical magnetic actuators with a center hole, i.e. - the geometry of magnetic thrust bearings, [3]. However, the full analytic model for cylindrical geometries developed by Zhu has not been previously extended for magnetic thrust bearing geometries. Here, the full analytic model developed by Zhu et al. is extended to allow for geometries with a center hole. The analytic model for thrust bearing geometries is then approximated in a transfer function form suitable for control design. The frequency responses for the full order and approximate models are compared to that of a finite element model for several bearing geometries. These results are also compared to the approximate model developed by Sun et al.

II. ANALYTICAL MODEL OF A CONVENTIONAL THRUST AMB

Zhu et al. developed an extensive 2-D magnetic circuit model of non-laminated axisymmetric actuators based on the ideas of skin effect and effective reluctance [1], [2]. Eddy current-induced skin effect describes the tendency for electromagnetic waves to travel near the surface of conductors. The depth at which the flux amplitude is reduced by $1/e \approx 1/3$ is the skin depth and is given by $\delta = 1/\sqrt{\pi f \mu_r \mu_0 \sigma}$ [1], [4], where μ_r is the magnetic permeability of the material relative to that of free space, μ_0, and σ is the conductance of the material. Neglecting the effects of eddy currents, the reluctance along a solid uniform material of length l and cross-sectional area A, is given by

$$R = \frac{l}{\mu_r \mu_o A} \tag{1}$$

However, in a solid magnetic actuator with eddy current effects, the cross-sectional area for varying flux is effectively reduced with increasing frequency, consistent with the skin effect, giving rise to the idea of effective permeability and effective reluctance [1], [2]. Using this idea Zhu et al. developed a magnetic circuit model with reluctance elements, dependent on the frequency of the current input that accurately captured the effects of eddy currents with a simple magnetic circuit model. The result of this work was a simple fractional order transfer function model of flux across the air gap (φg) with respect to perturbation current (ip) of the form:

$$\frac{\phi_g(s)}{i_p(s)} = \frac{N}{c\sqrt{s}+R^o} \tag{2}$$

where the denominator represents the effective reluctance of the circuit with static coefficient R^0 and dynamic coefficient c [1], [2]. Zhu et al. examined the dynamics of axisymmetric actuators without a center hole. Fig. 1 shows how the axisymmetric geometry may be defined using polar coordinates. The geometry may be divided into six regions as shown in Fig. 3. Reluctance models for each region were derived in [1], [2]. Only Regions 1 and 6 are effected by the presence of a center hole, i.e. $r_0 > 0$, so the reluctance models for these regions only, are rederived below for $r_0 > 0$. Reluctance networks used to derive the other reluctance models are described in detail in [2]. Early models of solid magnetic actuators assumed that flux density in the air gap was homogeneous. However, due to eddy current effects, the flux density in solid actuators varies across the air gap. For an axisymmetric geometry with cross section shown in Fig. 1 (axis of symmetry is the z-axis) flux density varies with radial position along the air gap. Fig. 2 shows flux density in the air gap predicted by finite element analysis (FEA), for an example

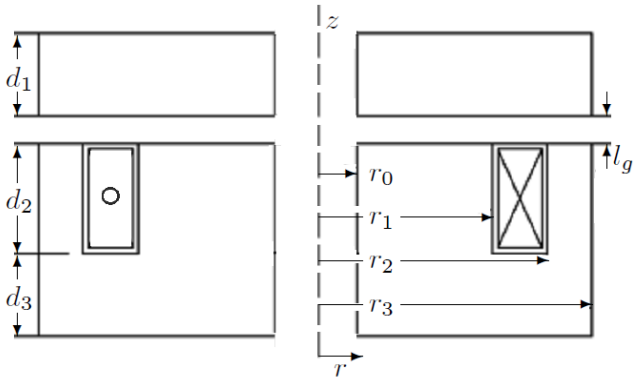

Figure 1. Parameters describing axisymmetric geometry of a magnetic thrust bearing.

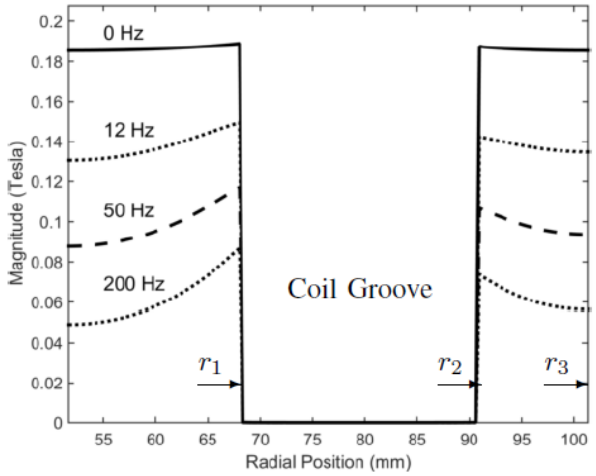

Figure 2. Air gap flux density varies with radial position.

actuator, beginning at the inner radius, r_0 = 51.7mm and moving towards the outer radius, r_3 = 101.3mm. Moving towards the outer radius across the inner pole, flux density increases. Flux fringing and leakage across the coil were neglected in this analysis so the flux density in the center hole, $r < r_0$, and coil groove, $r_1 < r < r_2$, is zero. Moving out across the outer pole, $r_2 < r < r_3$, flux density decreases. This variation of flux density across the pole face is an important aspect of actuator behavior that must be captured in high fidelity models.

A. Development of Analytic Model

Following the procedure used by Zhu [1], [2], the effective reluctance for Region 1 with a center hole is developed first. Based on the reluctance network and circuit theory, the magnetomotive force at a radial position, r, in the flotor, $F_{Mfl}(r)$, is given by the total magnetomotive force, F_M, minus the loss in magnetomotive force along the stator such that

$$F_{Mfl}(r) = F_M - F_{Mst}(r) \tag{3}$$

where F_M is the magnetomotive force equal to the number of coil turns, N, times the coil current, i. From the reluctance network for Region 1, Zhu et al. developed the following ordinary differential equation [2]:

$$\frac{d^2F_{Mst}(r)}{dr^2} + \frac{1}{r}\frac{dF_{Mst}(r)}{dr} - \alpha_1^2 F_{Mst}(r) = -\frac{\alpha_1^2}{2}F_M \tag{4}$$

where $\alpha = \sqrt{s\sigma\mu_r\mu_0}$ and $\alpha_1 = \sqrt{\frac{2\alpha}{\mu_r l_g}}$ (5)

(4) is a modified Bessel equation with the complete solution shown in (6).

$$F_{Mst}(r) = \frac{F_M}{2} + C_1 I_0(\alpha_1 r) + C_2 K_0(\alpha_1 r) \tag{6}$$

where $I_n(\cdot)$ is the nth-order modified Bessel function of the first kind and $K_n(\cdot)$ is the nth-order modified Bessel function of the second kind. Substitution of (3) into (6) yields

$$F_{Mfl}(r) = \frac{F_M}{2} - C_1 I_0(\alpha_1 r) - C_2 K_0(\alpha_1 r) \tag{7}$$

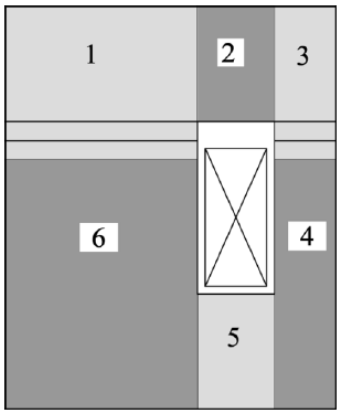

Figure 3. Axisymmetric geometry divided into six regions, each with an effective reluctance dependent on frequency.

For $r_0 > 0$, i.e. a geometry with a center hole, $F_{Mst}(r_1) = F_M$ and $\left.\frac{dF_{Mst}}{dr}\right|_{r=r_0} = 0$, C_1 and C_2 are given as follows:

$$C_1 = \frac{1}{2}\frac{F_M K_1(\alpha_1 r_0)}{I_1(\alpha_1 r_0)K_0(\alpha_1 r_1)+I_0(\alpha_1 r_1)K_1(\alpha_1 r_0)}, \text{and}$$

$$C_2 = \frac{1}{2}\frac{F_M I_1(\alpha_1 r_0)}{I_1(\alpha_1 r_0)K_0(\alpha_1 r_1)+I_0(\alpha_1 r_1)K_1(\alpha_1 r_0)} \tag{8}$$

Substituting (8) into (6) and (7) results in two equations for magnetomotive force at the surface of the stator, F_{Mst}, and flotor, F_{Mfl}, in the air gap as a function of radial position r:

$$F_{Mst}(r) = \frac{F_M}{2}\left[1 + \frac{I_0(\alpha_1 r)K_1(\alpha_1 r_0)}{I_1(\alpha_1 r_0)K_0(\alpha_1 r_1)+I_0(\alpha_1 r_1)K_1(\alpha_1 r_0)} + \frac{K_0(\alpha_1 r)I_1(\alpha_1 r_0)}{I_1(\alpha_1 r_0)K_0(\alpha 1_1 r_1)+I_0(\alpha_1 r_1)K_1(\alpha_1 r_0)}\right] \text{ and}$$

$$F_{Mfl}(r) = \frac{F_M}{2}\left[1 - \frac{I_0(\alpha_1 r)K_1(\alpha_1 r_0)}{I_1(\alpha_1 r_0)K_0(\alpha_1 r_1)+I_0(\alpha_1 r_1)K_1(\alpha_1 r_0)} - \frac{K_0(\alpha_1 r)I_1(\alpha_1 r_0)}{I_1(\alpha_1 r_0)K_0(\alpha_1 r_1)+I_0(\alpha_1 r_1)K_1(\alpha_1 r_0)}\right] \tag{9}$$

The flux density in the air gap,

$$B_g(r) = \frac{\mu_0}{l_g}\left(F_{Mst}(r) - F_{Mfl}(r)\right) \tag{10}$$

[2], may then be evaluated as:

$$B_g(r) = \frac{\mu_0 F_M}{l_g}\left(\frac{K_1(\alpha_1 r_0)I_0(\alpha_1 r)+I_1(\alpha_1 r_0)K_0(\alpha_1 r)}{I_1(\alpha_1 r_0)K_0(\alpha_1 r_1)+I_0(\alpha_1 r_1)K_1(\alpha_1 r_0)}\right) \tag{11}$$

Solving for the total flux in the air gap for Region 1 is achieved by integrating $B_g(r)$ from r_0 to r_1:

$$\phi_g = \int_{r_0}^{r_1} B_g(r) * 2\pi r\, dr = \frac{2\pi\mu_0 r_1 F_M}{l_g \alpha_1}\left(\frac{I_1(\alpha_1 r_1)K_1(\alpha_1 r_0) - I_1(\alpha_1 r_0)K_1(\alpha_1 r_1)}{I_1(\alpha_1 r_0)K_0(\alpha_1 r_1) + I_0(\alpha_1 r_1)K_1(\alpha_1 r_0)}\right) \quad (12)$$

Utilizing the relationship between magnetic flux in the air gap, φ_g, magnetomotive force, F_M, and reluctance, R, given by:

$$\phi_g = \frac{F_M}{R} \quad (13)$$

the effective reluctance for Region 1 can be expressed as:

$$R_1(s) = \frac{l_g \alpha_1}{2\pi\mu_0 r_1}\left(\frac{I_1(\alpha_1 r_0)K_0(\alpha_1 r_1) + I_0(\alpha_1 r_1)K_1(\alpha_1 r_0)}{I_1(\alpha_1 r_1)K_1(\alpha_1 r_0) - I_1(\alpha_1 r_0)K_1(\alpha_1 r_1)}\right) \quad (14)$$

For the static case, the reluctance should be determined by the air gap alone as eddy currents are absent. Indeed, the result obtained by taking the limit of $R_1(s)$ as the complex variable s approaches zero yields

$$R_1^0 = \lim_{s\to 0} R_1(s) = \frac{l_g}{\pi\mu_0(r_1^2 - r_0^2)} \quad (15)$$

which is the expected result. In addition, for $r_0 = 0$, the solution matches that obtained by Zhu et al. for the static reluctance of Region 1 [1]. The development of the effective reluctance model for Region 6 with $r_0 > 0$ is slightly different than that for Region 1. However, it is similar to the development of the effective reluctance of Region 4 described by Zhu et al. [2]. For Region 6, the reluctance network is formed by a series of parallel reluctances described by the ordinary differential equation

$$\frac{d^2 H_z}{dr^2} + \frac{1}{r}\frac{dH_z}{dr} - \alpha^2 H_z = 0 \quad (16)$$

the solution to which is given by:

$$H_z(r) = C_1 I_0(\alpha r) + C_2 K_0(\alpha r) \quad (17)$$

[2]. For Region 6 with $r_0 > 0$, the boundary conditions are $H_z(r_1) = H_{sf}$ and $dH_z(r)/dr\,|_{r=r0} = 0$, and the constants are:

$$C_1 = \frac{H_{sf} K_1(\alpha r_0)}{I_1(\alpha r_0)K_0(\alpha r_1) + I_0(\alpha r_1)K_1(\alpha r_0)}, \text{and}$$

$$C_2 = \frac{H_{sf} I_1(\alpha r_0)}{I_1(\alpha r_0)K_0(\alpha r_1) + I_0(\alpha r_1)K_1(\alpha r_0)} \quad (18)$$

where H_{sf} is the magnetic field strength at the actuator surface. It then follows that

$$H_z(r) = H_{sf}\frac{I_1(\alpha r_0)K_0(\alpha r) + K_1(\alpha r_0)I_0(\alpha r)}{I_0(\alpha r_1)K_1(\alpha r_0) + K_0(\alpha r_1)I_1(\alpha r_0)} \text{ and} \quad (19)$$

$$\mu_{eff}(r) = \mu_r\mu_0\frac{I_1(\alpha r_0)K_0(\alpha r) + K_1(\alpha r_0)I_0(\alpha r)}{I_0(\alpha r_1)K_1(\alpha r_0) + K_0(\alpha r_1)I_1(\alpha r_0)} \quad (20)$$

Effective reluctance for Region 6 is then

$$R_6(s) = \frac{d_2}{\int_{r_0}^{r_1}\mu_{eff}(r) * 2\pi r dr}$$

$$= \frac{d_2\alpha}{2\pi\mu_0\mu_r r_1}\frac{I_0(\alpha r_1)K_1(\alpha r_0) + I_1(\alpha r_0)K_0(\alpha r_1)}{I_1(\alpha r_1)K_1(\alpha r_0) - I_1(\alpha r_0)K_1(\alpha r_1)} \quad (21)$$

with static reluctance given by

$$R_6^0 = \lim_{s\to 0} R_6(s) = \frac{d_2}{\pi\mu_r\mu_0(r_1^2 - r_0^2)} \quad (22)$$

which, as expected, matches Zhu's result for $r_0 = 0$ [1].

B. Simplified Model of Solid Thrust AMB

The transcendental functions in the analytic model presented above are not suitable for control design. Therefore, a simplified analytic model for $R_1(s)$ and $R_6(s)$ with rational functions, is developed in this section. Taylor series and ad hoc approximations of $R_i(s)$ were compared to determine which method better represents the full reluctance model. The Taylor series (TS) and ad hoc (AH) reluctance approximations for Regions 1 and 6 with $r_0 > 0$ are given by

$$R_1^{TS}(s) = \frac{l_g}{\pi\mu_0(r_1^2 - r_0^2)} + \frac{2r_0^4 log\frac{r_1}{r_0} + \frac{3}{2}r_0^4 - 2r_1^2 r_0^2 + \frac{1}{2}r_1^4}{2\pi(r_1^2 - r_0^2)^2}\sqrt{\frac{\sigma}{\mu_r\mu_0}}\sqrt{s}$$

$$R_1^{AH}(s) = \frac{l_g}{\pi\mu_0(r_1^2 - r_0^2)} + \frac{\sqrt{2}}{2\pi r_1}\sqrt[4]{\frac{\sigma g^2}{\mu_r\mu_0^3}}\sqrt[4]{s}$$

$$R_6^{TS}(s) = \frac{d_2}{\pi\mu_r\mu_0(r_1^2 - r_0^2)} + \frac{d_2}{2\pi}\frac{2r_0^4 log\frac{r_0}{r_1} + \frac{3}{2}r_0^4 - r_0^2 r_1^2 + \frac{1}{2}r_1^4}{(r_1^2 - r_0^2)^2}\sigma s, \text{ and}$$

$$R_6^{AH}(s) = \frac{d_2}{\pi\mu_r\mu_0(r_1^2 - r_0^2)} + \frac{d_2}{2\pi r_1}\sqrt{\frac{\sigma}{\mu_r\mu_0}}\sqrt{s} \quad (23)$$

Ad hoc and Taylor series approximations were compared to the full analytic model in reference [5] where it was found that the Taylor series matched the magnitude and phase of the full model more closely for Region 1. For Region 6, the ad hoc approximation was found to match the full analytic model better in both magnitude and phase [5]. Effective reluctances for Regions 1 and 6 are shown in Table I along with the proposed approximations. For Regions 2 through 5, the reluctance models that will be used for analysis here are the same as those found in [1], [2] and are included in Table II for completeness.

Table I. Effective reluctances, $R_i(s)$, for Regions 1 and 6

Region	Full Model
1 ($r_0 > 0$)	$\frac{l_g\alpha_1}{2\pi\mu_0 r_1}\frac{I_1(\alpha_1 r_0)K_0(\alpha_1 r_1) + I_0(\alpha_1 r_1)K_1(\alpha_1 r_0)}{I_1(\alpha_1 r_1)K_1(\alpha_1 r_0) - I_1(\alpha_1 r_0)K_1(\alpha_1 r_1)}$
6 ($r_0 > 0$)	$\frac{d_2\alpha}{2\pi\mu_0\mu_r r_1}\frac{I_0(\alpha r_1)K_1(\alpha r_0) + I_1(\alpha r_0)K_0(\alpha r_1)}{I_1(\alpha r_1)K_1(\alpha r_0) - I_1(\alpha r_0)K_1(\alpha r_1)}$

Region	Approximate
1 ($r_0 > 0$)	$\frac{l_g}{\pi\mu_0(r_1^2 - r_0^2)} + \frac{2r_0^4\log\frac{r_1}{r_0} + \frac{3}{2}r_0^4 - 2r_1^2r_0^2 + \frac{1}{2}r_1^4}{2\pi(r_0^2 - r_1^2)^2}\sqrt{\frac{\sigma}{\mu_r\mu_0}}\sqrt{s}$
6 ($r_0 > 0$)	$\frac{d_2}{\pi\mu_r\mu_0(r_1^2 - r_0^2)} + \frac{d_2}{2\pi r_1}\sqrt{\frac{\sigma}{\mu_r\mu_0}}\sqrt{s}$

$\alpha_1 = \sqrt{\frac{2\alpha}{\mu_r g}}$, $\alpha = \sqrt{s\sigma\mu_0\mu_r}$

Table II. Effective reluctances, Ri(s), for Regions 2 through 5 of axisymmetric geometry [1].

Region	Full Model
2	$\frac{\ln(r2/r1)}{2\pi\mu_r\mu_0}\frac{\alpha}{\tanh(\alpha d_1)}$
3	$\frac{l_g\alpha_1}{2\pi\mu_0 r_2}\frac{I_0(\alpha_1 r_2)K_1(\alpha_1 r_3)+K_0(\alpha_1 r_2)I_1(\alpha_1 r_3)}{K_1(\alpha_1 r_2)I_1(\alpha_1 r_3)-I_1(\alpha_1 r_2)K_1(\alpha_1 r_3)}$
4	$\frac{d_2\alpha}{2\pi\mu_r\mu_0 r_2}\frac{I_0(\alpha r_2)K_1(\alpha r_3)+K_0(\alpha r_2)I_1(\alpha r_3)}{K_1(\alpha r_2)I_1(\alpha r_3)-I_1(\alpha r_2)K_1(\alpha r_3)}$
5	$\frac{\ln(r_2/r_1)}{2\pi\mu_r\mu_0}\frac{\alpha}{\tanh(\alpha d_3)}$

Region	Approximate $(R_i^0+c\sqrt{s})$
2	$\frac{\ln(r_2/r_1)}{2\pi\mu_r\mu_0 d_1}+\frac{\ln(r_2/r_1)}{2\pi}\sqrt{\frac{\sigma}{\mu_r\mu_0}}\sqrt{s}$
3	$\frac{l_g}{\pi\mu_0(r_3^2-r_2^2)}+\frac{\left(2r_3^4\log\frac{r_3}{r_2}-\frac{3}{2}r_3^4+2r_2^2r_3^2-\frac{1}{2}r_2^4\right)}{2\pi(r_3^2-r_2^2)^2}\sqrt{\frac{\sigma}{\mu_r\mu_0}}\sqrt{s}$
4	$\frac{d_2}{\pi\mu_r\mu_0(r_3^2-r_2^2)}+\frac{d_2}{2\pi r_2}\sqrt{\frac{\sigma}{\mu_r\mu_0}}\sqrt{s}$
5	$\frac{\ln(r_2/r_1)}{2\pi\mu_r\mu_0 d_3}+\frac{\ln(r_2/r_1)}{2\pi}\sqrt{\frac{\sigma}{\mu_r\mu_0}}\sqrt{s}$

C. Comparison with Finite Element Analysis

To verify the accuracy of the analytic models developed in the previous section, several test cases were chosen for examination. The first test case is similar to an existing thrust bearing on a compressor surge test rig developed at the University of Virginia [6], [7]. Several other test cases were derived by modifying the geometric properties of this bearing as summarized in Table III. FEA was performed using Finite Element Method Magnetics (FEMM) [8] over a range of current excitation frequencies from static to 400Hz. Flux magnitude and phase were plotted to determine the minimal mesh resolutions required (Fig. 4). Flux magnitudes were similar for each of the mesh resolutions tested using FEMM (Fig. 4). However, for the lowest resolution mesh, the phase diverged from that of the finer meshes for frequencies above 100Hz (Fig. 4). At higher frequencies the eddy-current induced skin effect restricts the flux path to the surface region adjacent to the coil [1]. With the flux concentrated in fewer elements near the surface, and a steep flux gradient at the edge of this region, a finer mesh resolution is required in order to obtain accurate results. The highest mesh resolution (6 million nodes for Case 1) was used for all subsequent finite element analysis performed using FEMM. Flux magnitudes and phase for several geometries were predicted using the full model presented above as well as the approximate analytic model developed from it. These were compared to predictions from FEA that excluded flux leakage and fringing (Figs. 5 - 7). Flux magnitudes for each model were normalized to the static results of the FEA model:

$$M_{norm} = 20log\left|\frac{G_i(j\omega)}{G_0(0)}\right| \quad (24)$$

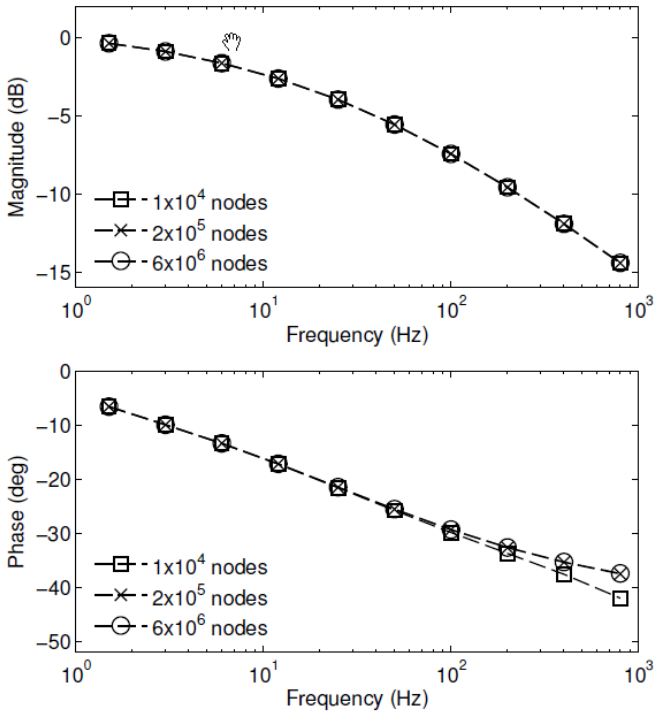

Figure 4. 2-D finite element modeling shows the flux magnitude and phase for three mesh resolutions.

where M_{norm} is the normalized flux magnitude in dB, $G_i(j\omega)$ represents the model data being normalized, and $G_0(0)$ is the static response of the FEA model without leakage or fringing. The full analytic model agreed closely with the FEA model. Furthermore, in most cases the approximate model's frequency response closely matched the FEA results. The approximate models yielded similar results with the maximum difference in magnitude of 0.230dB and a maximum difference in phase of 0.539 deg for all six cases.

Table III. Maximum multiplicative error (ME) of flux magnitude computed using the model derived above and the model from Sun et al., relative to FEA without leakage and fringing.

Case	Full Model Max ME (%)	Approximate Max ME (%)	Sun et al. Max ME (%)
1	27.5	7.44	7.73
2	21.9	4.15	4.32
3	21.9	9.02	9.3
4	45.9	10.6	10.9
5	23.8	6.38	6.29

Table IV shows the maximum multiplicative error (ME),

$$ME(f) = \frac{|G_{f(x)}(f)-G_{FEA}(f)|}{|G_{FEA}(0)|}100\% \quad (25)$$

relative to FEA for the approximate model developed here, and the Sun et al. model. The maximum MEs for the two approximate models were similar reflecting the close agreement in frequency response predicted by each approximation. The greatest ME was 10.6% for the approximation developed above and 10.9% for the

approximation reported by Sun et al.. Both of these were observed for case 4 and both occurred at low frequency, 1.5Hz.

Table V shows the maximum phase error (PE),

$$PE(f) = \angle G_{f(x)}(f) - \angle G_{FEA}(f) \qquad (26)$$

for both approximations. Both approximations resulted in very small phase error with the largest errors observed for Case 4 which are less than 2 deg. Larger errors observed for Case 4 are also seen in for the full analytic model and are likely due to the inability of the full analytic model to capture the eddy current effects of a geometry with a deep coil groove, rather than a divergence of the full and approximate analytic models for this geometry. Frequency response plots of three representative cases are included in Figures 5 through 7. For Case 2 the approximate model performed best in capturing the FEA behavior as evidenced by the small error in flux magnitude. For Case 4, the approximate model had the largest error in flux magnitude that was seen in our investigation. The full model developed herein performed very well for all geometries. In all cases examined, the differences in results between our approximate model and that developed by Sun et al. was negligible in both magnitude and phase, suggesting that both approximate models are equally valid. The Sun approximate model has the advantage of a simpler analytic expression.

Table IV. Maximum absolute value of phase error (PE) of flux computed using the model derived above and the model from Sun et al., relative to FEA without leakage and fringing.

Case	Full Model Max PE (deg)	Approximate Max PE (deg)	Sun et al. Max PE (deg)
1	3.65	1.64	1.42
2	3.67	0.967	0.9
3	2.78	1.73	1.57
4	5.22	1.98	1.84
5	3.69	1.56	1.47
6	3.53	1.52	1.27

Table V. -3dB and -15 deg bandwidths computed for FEA, full and approximate models.

Case	FEA -3 dB (Hz)	Full Model -3 dB (Hz)	Approx. -3 dB (Hz)	FEA -15 deg (Hz)	Full Model -15 deg (Hz)	Approx. -15 deg (Hz)
1	15	26.6	10.8	8.12	14.4	9.18
2	44.6	79.8	36.8	31.4	57.7	33.8
3	10.8	16.9	7.3	5.41	8.06	6.28
4	8.77	20.9	5.59	3.93	8.82	4.77
5	37.8	68.4	28.4	22.5	40.7	25.3
6	7.27	12.6	5.06	3.51	6.06	3.92

III. DISCUSSION

The transfer function model developed by Sun et al. [3] was developed by extending the simplified model developed by Zhu et al. [1], [2] for an inner radius greater than zero. In the process, the magnetic circuit model developed was

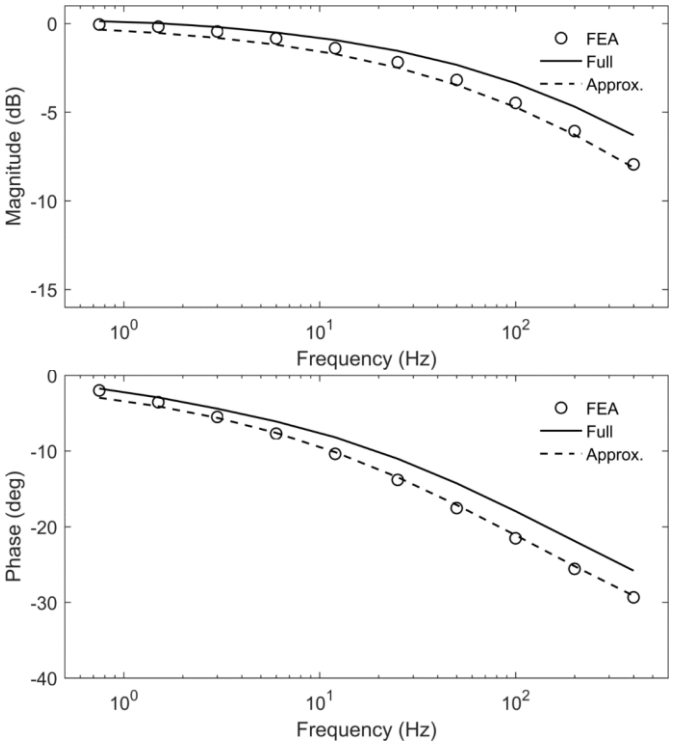

Figure 5. Case 2 (1mm air gap): Normalized flux magnitude and phase predicted by FEA model without flux leakage or fringing (FEA), full analytic model, and simplified analytic model (Approx.).

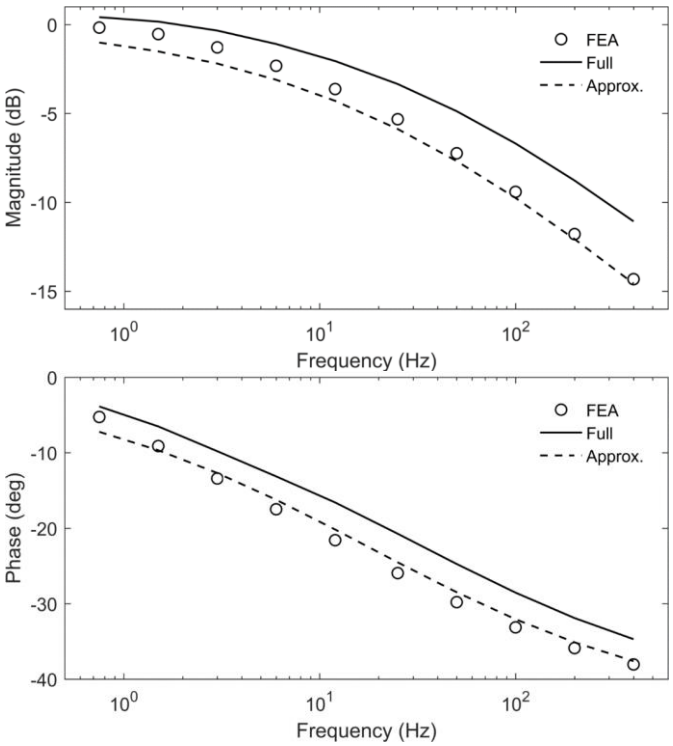

Figure 6. Case 4 (deep coil groove): Normalized flux magnitude and phase predicted by FEA model without flux leakage or fringing (FEA), full analytic model, and simplified analytic model (Approx.).

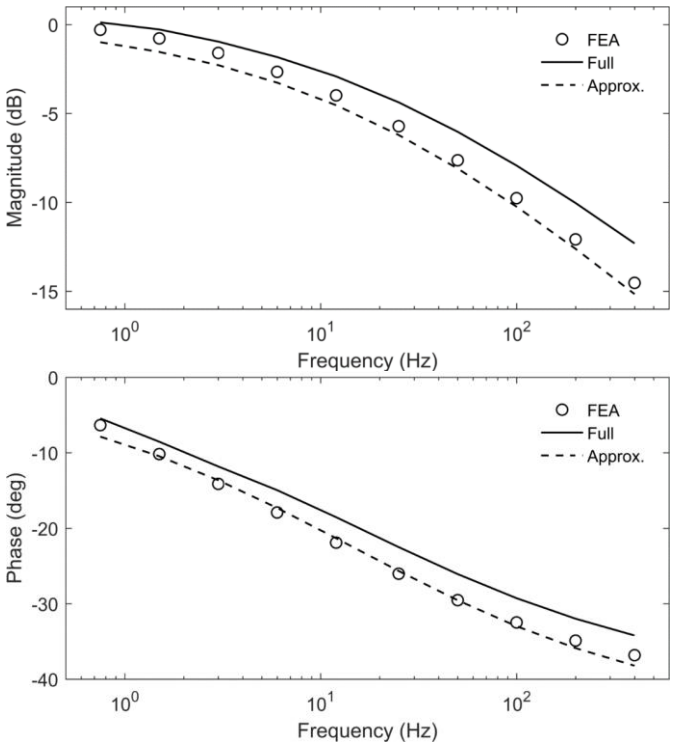

Figure 7. Case 6 (small inner radius): Normalized flux magnitude and phase predicted by FEA model without flux leakage or fringing (FEA), full analytic model, and simplified analytic model (Approx.).

modified from the original form and the full analytic model was not considered. In this work the development of analytic models is carried out by extending the full analytic model for solid cylindrical electromagnetic actuators to included cases where the inner radius is greater than zero using the same magnetic circuit model. With the full analytic model defined for this new geometry, a simplified model was developed using Taylor series and ad hoc approximations. By comparison to FEA results it is shown that both the full model and the approximate model provide useful predictions of actuator frequency response. The approximate model, however, is substantially better than the full model in predicting actuator bandwidth. Bandwidths predicted using the approximate model were similar to those predicted by the Sun model.

IV. CONCLUSIONS

Analytic models for solid thrust AMBs were developed by extending the work of Zhu et al. on modeling of solid cylindrical electromagnetic actuators [1], [2]. Modification of the boundary conditions for Zhu's axisymmetric model led to the full analytic model for axisymmetric geometries with a center hole, i.e. having the geometry of a thrust AMB. An approximate analytic model was also developed using Taylor Series and ad hoc approximation methods. The frequency response of the full analytic model was found to agree closely with FEA results. The approximate model developed here also performed extremely well and similar to that developed in [3].

ACKNOWLEDGMENT

The authors would like to thank David Meeker for making FEMM freely available and for helpful advice with FEA. Thanks to Lei Zhu as well for helpful input regarding FEA. Finally, we would like to thank the Rotating Machinery and Controls (ROMAC) Laboratory at the University of Virginia, which provided the funding for this work.

REFERENCES

[1] L. Zhu, C. Knospe, and E. Maslen, "Analytic model for a nonlaminated cylindrical magnetic actuator including eddy currents", IEEE Transactions on Magnetics, vol. 41, no. 4, pp. 1248–1258, 2005.

[2] L. Zhu, "Non-laminated magnetic actuators: Modeling and performance limitations", PhD thesis, University of Virginia, 2005.

[3] L. Y. Yanhua Sun Yick-Sing Ho, "Dynamic stiffness of active magnetic thrust bearing including eddy-current effects", IEEE Transaction on Magnetics, vol. 45, no. 1, 2009.

[4] D. J. Griffiths, Introduction to Electrodynamics. PrenticeHall, 1989.

[5] Z. W. Whitlow, "Modeling and control of non-laminated active magnetic thrust bearings", Master's thesis, University of Virginia, 2014.

[6] S. Y. Yoon, "Surge control of active magnetic bearing suspended centrifugal compressors", PhD thesis, University of Virginia, 2011.

[7] S. Yoon, Z. Lin, and P. Allaire, Control of Surge in Centrifugal Compressors by Active Magnetic Bearings. Springer, 2013.

[8] D. C. Meeker, Finite element method magnetics. Version 4.2 (11Apr2012), [Online]. Available: http:// www.femm.info/wiki/HomePage.